

PCCP

Accepted Manuscript



This is an *Accepted Manuscript*, which has been through the Royal Society of Chemistry peer review process and has been accepted for publication.

Accepted Manuscripts are published online shortly after acceptance, before technical editing, formatting and proof reading. Using this free service, authors can make their results available to the community, in citable form, before we publish the edited article. We will replace this *Accepted Manuscript* with the edited and formatted *Advance Article* as soon as it is available.

You can find more information about *Accepted Manuscripts* in the [Information for Authors](#).

Please note that technical editing may introduce minor changes to the text and/or graphics, which may alter content. The journal's standard [Terms & Conditions](#) and the [Ethical guidelines](#) still apply. In no event shall the Royal Society of Chemistry be held responsible for any errors or omissions in this *Accepted Manuscript* or any consequences arising from the use of any information it contains.

Stability of Pt near surface alloys under electrochemical conditions: a model study

Xiaoming Zhang,¹ Shansheng Yu¹, Weitao Zheng^{1*} and Ping Liu^{2*}

¹Department of Materials Science, Key Laboratory of Mobile Materials, MOE, and State Key Laboratory of Superhard Materials, Jilin University, Changchun 130012, PR China.

²Center for Functional Nanomaterials, Brookhaven National Laboratory, NY 11973, USA

Abstract

The stability is one of the key requirements for commercializing the fuel cell electrocatalysts in automotive applications. For the widely used Pt-based catalysts, it can be achieved by the formation of a stable Pt skin on the surface. Here, we employed density functional theory (DFT) to explore the stability of monolayer Pt (Pt_{ML}) on various near surface alloy (NSAs) surfaces, $\text{Pt}_{\text{ML}}/\text{M}_{\text{ML}}/\text{Pt}(111)$ ($\text{M}=\text{Fe}, \text{Co}, \text{Ni}, \text{Cu}; \text{Ru}, \text{Rh}, \text{Pd}, \text{Ag}; \text{Os}, \text{Ir}, \text{Au}$), under various environments. Our results show that under the vacuum condition, the alloying M except Ag and Au thermodynamically prefer to stay in the subsurface and the formation of Pt_{ML} on the surface is thermodynamically favored. A barrier has to be overcome for M to segregate. The situation varies under various electrochemical conditions. Depending on the solutions and the operating reaction pathway, different M should be considered for alloying with Pt to maintain the stability of surface Pt_{ML} . PtRh and PtPd are the only two systems, where the surface Pt_{ML} is likely to stay intact under perchloric acid (HClO_4), sulfuric acid (H_2SO_4), phosphoric acid (H_3PO_4) and alkaline solutions as well as under the oxygen reduction reaction (ORR) conditions via different pathways. PtIr should also be paid attention, which falls only during the ORR via the OOH intermediate. Our results highlight the importance of chemical environments in affecting the stability of the catalysts.

Keywords: Near surface alloy, Acid/Alkaline solution, Stability, ORR, DFT

* Corresponding authors: Weitao Zheng, wzhen@jlu.edu.cn & Ping Liu, pingliu3@bnl.gov

1. Introduction

The low-temperature fuel cell is one of the most promising clean energy technologies, particularly attractive for automobile applications due to their high efficiency, high energy density, and low or zero emissions(1; 2). However, several problems have hindered the commercialization (3-9). One of the challenges is the slow kinetics of the oxygen reduction reaction (ORR) at the cathodes that causes a large loss of the cell voltage. As a consequence, a significant efficiency loss occurs, which is mitigated by use of large amounts of expensive Pt catalyst. Recently, considerable advances have been made by forming Pt alloys with a monolayer Pt on the surface (Pt_{ML}), being able to accelerate the ORR and reduce the Pt loading (10-13). Extensive theoretical studies have been carried out to understand their superior ORR activities, which provide the key for rational design of better catalysts. (14-20) In contrast, less attention has been made for the stability of Pt_{ML} shell,(12; 21; 22) which is critical to achieve the catalyst durability required for commercializing fuel cell in automotive applications. A systematic theoretical study was reported on the stability of Pt_{ML} on various metal surfaces; (23) yet the harsh operating conditions of fuel cell were not considered, which might induce the segregation of core metals to the surface. As a result, the activity varies and the stability decreases.(22; 24; 25)

Here we employed density functional theory (DFT) to study the segregation of core metals under various environments. To model the core-shell nanoparticles, we used the near surface alloys (NSAs) as a model system, where 1ML of M (M=Fe, Co, Ni, Cu, Ru, Rh, Pd, Ag, Os, Ir, Au) was incorporated into the subsurface of single crystal of Pt(111) and formed the $\text{Pt}_{\text{ML}}/\text{M}_{\text{ML}}/\text{Pt}(111)$ sandwich structure. In both theoretical and experimental studies, NSAs have been used not only as effective models to simulate metal alloy nanoparticles, but also as an advanced method to improve the catalytic activity for heterogeneous catalysis (e.g. hydrogenation reaction and water-gas shift reaction) and electrocatalysis in fuel cells (e.g. hydrogen oxidation, CO oxidation and oxygen reduction reactions). (26-33) Of course, NSAs are model catalysts with the more

ideal than the practical powder catalysts. However, according to the previous studies, (26-28; 31) the trend we presented here from one NSA to the next can be of great importance to the catalyst development for practical applications. Ideally, to achieve the reasonable stability, the formation of Pt_{ML} on the surface is preferred. The segregation of active M to the surface can facilitate the surface oxidation and therefore the dissolution of the Pt catalyst.(13; 34) Our calculations show that the surface structure of a NSA can be strongly dependent on the working environment. Depending on the solutions and the operating pathway of the ORR, different alloying M should be considered for the Pt-based catalysts to achieve the stability of surface Pt_{ML} .

2. Methods and models

Spin-polarized DFT calculations were performed using the CASTEP code(35; 36). The generalized gradient approximation (GGA)(37) with the revised Perdew–Burke–Ernzerhof functional (RPBE)(38) was used to describe the exchange and correlation potential. The cutoff energy for the plane-wave basis set was set to 520 eV in all calculations. The Monkhorst-Pack (39) mesh k-points ($9 \times 9 \times 9$) and ($5 \times 5 \times 1$) were used for the bulk and slab calculations, respectively. A convergence accuracy of $1.0 \times 10^{-6} eV/atom$ was set for the self-consistent field (SCF) calculation. In our DFT calculations, the NSAs, $Pt_{ML}/M_{ML}/Pt(111)$ (M=Fe, Co, Ni, Cu, Ru, Rh, Pd, Ag, Os, Ir, Au) were modeled with a five-layer slab using a 2×2 supercell (Figure 1a). In addition, the gradual segregation of M from the subsurface to form $Pt_3M_1/Pt_1M_3/Pt(111)$, $Pt_2M_2/Pt_2M_2/Pt(111)$, $Pt_1M_3/Pt_3M_1/Pt(111)$ and eventually $M_4/Pt_4/Pt(111)$ was considered. A vacuum gap of 15 Å in the z-direction was introduced to separate two subsequent slabs. The atoms in the top three layers were allowed to relax, while the atoms on the remaining two layers were fixed at their ideal bulk positions.

The adsorption energies of *O, *OH, *OOH, *ClO₄, *SO₄ and *PO₄ at different adsorption sites were examined at 0.25 ML. The segregation energy under different conditions was calculated by

$$\Delta E_{\text{segr}}(i) = E_{\text{ads+Pt}_{4-i}\text{M}_i/\text{Pt}_i\text{M}_{4-i}/\text{Pt}(111)} - E_{\text{ads+Pt}_4/\text{M}_4/\text{Pt}(111)},$$

where E is the total energy of the adsorbed slabs and i is the number of M atom in the surface layer ($0 \leq i \leq 4$). $\Delta E_{\text{segr}}(i)$ represents the energy cost for i M atoms segregating from the subsurface to the surface by exchanging position with nearby Pt atoms in the surface.

3. Results and discussions

3.1 Stability under vacuum conditions

We first calculated the segregation energy, $\Delta E_{\text{segr}}(i)$, of bare surfaces to estimate the stability of the NSAs under vacuum conditions, where our calculated $\Delta E_{\text{segr}}(1)$ agree well with the previous study.⁽⁴⁰⁾ As shown in Figure 2 and Table S1, for most of $\text{Pt}_{\text{ML}}/\text{M}_{\text{ML}}/\text{Pt}(111)$ studied $\Delta E_{\text{segr}}(i)$ is positive with $\Delta E_{\text{segr}}(4) > \Delta E_{\text{segr}}(3) > \Delta E_{\text{segr}}(2) > \Delta E_{\text{segr}}(1)$. It means that Pt energetically prefers to stay on the surface to form a Pt skin or Pt_{ML} , while M favors to stay in the subsurface ($\text{Pt}_4/\text{M}_4/\text{Pt}(111)$). The more M atoms are in the surface, the more energy will cost for M to segregate from the subsurface. The exceptions are PtAg and PtAu . An inverse order, $\Delta E_{\text{segr}}(4) < \Delta E_{\text{segr}}(3) < \Delta E_{\text{segr}}(2) < \Delta E_{\text{segr}}(1)$, is observed. This is associated with the lower surface energy of the surfaces terminated by Ag or Au than that by Pt .⁽⁴⁰⁾ In addition, a general trend between the calculated $\Delta E_{\text{segr}}(i)$ and individual M is observed. For instance, when M goes from Fe of group 8 to the right of the periodic table, Co of group 9, Ni of group 10 and Cu of group 11, the magnitude of $\Delta E_{\text{segr}}(4)$ decreases (Figure 2) from 3.86 eV to 3.05 eV, 2.33 eV and 1.59 eV, respectively. Similar trend is also observed for the 4d (from Ru to Ag) and 5d metals (from Os to Au). Along the same column, the Pt NSAs with the

3d M (Fe, Co, Ni, Cu) shows more significant variation in $\Delta E_{\text{segr}}(i)$ than those with 4d M (Ru, Rh, Pd, Ag) and 5d M (Os, Ir, Au), respectively. Such trend is associated with the d-band center (E_d) of M, which affects the adsorptions of various adsorbates on metal surfaces. (40) In general, from group 8 to group 11 metals and from 3d to 5d metals in the periodic table, M E_d shifts downward or away from the Fermi level. Extensive studies have shown that the higher E_d locates, the more active the corresponding M is and the higher the surface energy when M is on the surface. (40) $\Delta E_{\text{segr}}(i)$ shown in Figure 2 reflects the competition between Pt and M. In general, for M having E_d close to that of Pt (e.g. Pd, Figure S1), the corresponding $\Delta E_{\text{segr}}(i)$ for the NSA is much smaller in magnitude than that having E_d far away from Pt (e.g. Fe, Figure S1). Among the systems studied, the largest variation in $\Delta E_{\text{segr}}(i)$ is observed for the case of PtFe, where Fe displays the highest-lying E_d and therefore the highest activity among the M metals studied and $\Delta E_{\text{segr}}(4)$ (3.86 eV) \gg $\Delta E_{\text{segr}}(1\sim 3)$ (0.65 eV, 1.68 eV and 2.21 eV respectively). That is, there is a strong driving force for Fe to occupy the subsurface sites rather than the surface sites. It can be extremely difficult for Fe to segregate to the surface under vacuum conditions. In contrast, Pt₄/Pd₄/Pt(111) shows the least variation in $\Delta E_{\text{segr}}(i)$ (< 0.4 eV), suggesting a more facial shift of Pd between the surface and subsurface layers. Figure S1 shows that there is a linear-like correlation between M E_d of M_{ML}/Pt(111) and the corresponding $\Delta E_{\text{segr}}(4)$.

For practical applications in fuel cells, the formation of Pt_{ML} is preferred to achieve both the activity and stability. Accordingly, we scaled the stability of Pt_{ML} on a NSA surface using the lowest $\Delta E_{\text{segr}}(i)$, which can represent the lowest energy cost to allow segregation of M to the surface and therefore destabilize Pt_{ML}. As shown in Figure 3, under vacuum conditions Pt_{ML}/M_{ML}/Pt(111) (M=Fe, Co, Ni, Cu, Ru, Rh, Pd, Os, Ir) surfaces can be considered as good candidates, where the color index (blue to white) indicates the formation of Pt_{ML} on the surface is either exothermic (M=Fe, Co, Ni, Cu,

Ru, Rh, Os, Ir) or at least thermoneutral ($M = Pd$). Upon alloying with Ag and Au, $M_{ML}/Pt(111)$ is more favorable than the $Pt_{ML}/M_{ML}/Pt(111)$. Indeed, the small amount of Au on the surface of Pt or Pt alloy catalysts have been found to promote the stability of the catalysts effectively.^(22; 24) However, once the surface is fully covered by Ag or Au, the activity is likely to decrease, as Ag and Au are not as active as Pt for the ORR.⁽⁴¹⁾ Therefore, PtAg and PtAu alloys will not be considered for our further study in the following.

3.2 Stability under acidic and alkaline solutions.

The electrochemical environment is quite different from the vacuum, which typically are either acidic or alkaline. Can the stable $Pt_{ML}/M_{ML}/Pt(111)$ systems under vacuum conditions survive in the solutions? To answer that, three acids were included in our study ($HClO_4$, H_2SO_4 and H_3PO_4), where the adsorption of anion species on the surface was considered (Figure 4). Here we assume that the solvent effect on the anion species is independent of the composition of NSAs. In this way, the trend from one system to the next we reported here is likely to represent the case when the solvation is taken into consideration. As you will see below, the trend our calculations predicted for the structural effect of $HClO_4$, H_2SO_4 and H_3PO_4 agrees with the experimental observations. The effect of alkaline was simulated by OH adsorbed on the surfaces. On a $Pt_{ML}/M_{ML}/Pt(111)$, the possibility of sequentially pulling M from the subsurface out to the surface to form strong bonds with the adsorbates was also included (Figure 4).

According to our calculations, the tetrahedral $*ClO_4$ is anchored on the surfaces by three oxygen atoms at Pt atop sites in a η^3 conformation (Figure 4), in accordance with previous theoretical study.⁽⁴²⁾ One can see in Figure 5a that $*ClO_4$ -induced variation in $\Delta E_{segr}(i)$ is different from the case under the vacuum condition (Figure 2). First of all, the magnitude is decreased significantly on going from vacuum to $HClO_4$. Again, the E_d and therefore the activity of M play an essential in determining the observed trend in Figure 5a. For instance, among the systems studied, alloying with Fe leads to the most

significant changes in $\Delta E_{\text{segr}}(4)$ from 3.86 eV under the UHV conditions to 1.05 eV due to the presence of $^*\text{ClO}_4$. This is due to the fact that Fe has a much highest-lying d-band than the other M studied and therefore $^*\text{ClO}_4$ binds Fe the most strongly than the others including Pt, which provides a big driving force for Fe segregating back to the surface. However, it is only able to compensate in some degree the energy cost and Fe still prefers to stay in the subsurface. Besides PtFe, PtM (M = Co, Ni, Ru, Os, Ir) are in the similar situation. In another word, for these systems the $\text{Pt}_{\text{ML}}/\text{M}_{\text{ML}}/\text{Pt}(111)$ conformation is thermodynamically stable in HClO_4 solution. Among them, Os shows the strongest anti-segregation to the surface and therefore the most stable Pt skin on the surface of PtOs. In contrast, $\Delta E_{\text{segr}}(i)$ can be negative for PtM (M=Cu, Rh, Pd) (Figure 5a and Table S2). The stronger M- ClO_4 interaction than that of Pt- ClO_4 is able to compensate the segregation energy and stabilize M on the surface; yet thermodynamically the exothermicity is not strong (< 0.25 eV). Thus, the segregation may not be feasible under operating conditions of low-temperature fuel cells due to the kinetic obstacles and may only take place via the surface defect.(22) This is associated with the relatively moderate binding of tetrahedral $^*\text{ClO}_4$, which has been observed experimentally using a hanging-meniscus rotating-disk electrode, demonstrating small structural effects in HClO_4 solution.(43)

The tetrahedral $^*\text{SO}_4$ and $^*\text{PO}_4$ adopt the same conformation as that of $^*\text{ClO}_4$ (Figure 4), in consistent with the previous observations; (44; 45) however the induced changes in energetics and structures are different. There is an increasing in binding energy when going from $^*\text{ClO}_4$ to $^*\text{SO}_4$ and eventually $^*\text{PO}_4$, resulting in the further decreasing of $\Delta E_{\text{segr}}(i)$ (Figure 5b,c and Table S3,4). For instance, $\Delta E_{\text{segr}}(4)$ for PtFe decreased from 1.05 eV to 0.05 eV and -0.76 eV, respectively (Figure 5a,b,c). Such effect has been observed experimentally, showing a considerable effect of H_2SO_4 (46) and a pronounced effect of H_3PO_4 (47; 48) on the crystal structure of Pt catalysts in contrast to HClO_4 . In H_2SO_4 solution the $\text{Pt}_{\text{ML}}/\text{M}_{\text{ML}}/\text{Pt}(111)$ conformation are able to survive for most of alloys though it is not as stable as that in HClO_4 solution. As shown in Figure 5b,

$\Delta E_{\text{segr}}(i)$ are positive for PtOs and PtIr, while for the other PtM systems $\Delta E_{\text{segr}}(i)$ are almost thermoneutral (< 0.20 eV). Accordingly, the segregation of M is still not energetically favorable. In contrast, $\Delta E_{\text{segr}}(i)$ for PtCu is negative, though it is only around -0.3 eV. $^*\text{PO}_4$ promotes the segregation of M more strongly than $^*\text{SO}_4$ and $^*\text{ClO}_4$. As shown in Figure 5c, only PtNi, PtRh, PtPd and PtIr alloys are able to hold the Pt_{ML} on the surface; yet the value of $\Delta E_{\text{segr}}(i)$ is small (< 0.13 eV). For the other systems, the strong effects of $^*\text{PO}_4$ enable the segregation of active M to the surface thermodynamically favorable, among which the most negative $\Delta E_{\text{segr}}(i)$ is observed for PtFe ($\Delta E_{\text{segr}}(3) = -0.76$ eV).

Compared to the acid solutions, the effect of alkaline solutions is less significant. Again, the adsorption of OH on the surface with and without segregating M to the surface was considered. The preferential adsorption sites for OH vary from atop, bridge to hollow depend on the amount of M on the surface (Figure 6). Figure 5d (also see Table S5) shows that $^*\text{OH}$ species help to lower $\Delta E_{\text{segr}}(i)$ compared to the cases in vacuum; yet they still stay as positive. It indicates the preference to the $\text{Pt}_{\text{ML}}/\text{M}_{\text{ML}}/\text{Pt}(111)$ conformation, where the most positive $\Delta E_{\text{segr}}(i)$ is observed for PtOs with $\Delta E_{\text{segr}}(3) = 1.27$ eV. For PtCu, PtPd and PtOs, $\Delta E_{\text{segr}}(i)$ can be negative depending on the amount of M on the surface; however the values are very small (< 0.15 eV), which may not be practical to proceed under the reaction conditions of low-temperature fuel cells.

For all the systems studied in this section, M correspond to the higher-lying E_d and therefore are more active than Pt. These metals prefer to stay in the subsurface under vacuum conditions to form $\text{Pt}_{\text{ML}}/\text{M}_{\text{ML}}/\text{Pt}(111)$ (Figure 3). However, the situation varies by including the effect of solutions under the working condition of fuel cells. The interaction with the anion of the solutions drives $\Delta E_{\text{segr}}(i)$ less positive (Figure 3) and therefore helps to stabilize M segregated to the surface. In HClO_4 solution, the $\text{Pt}_{\text{ML}}/\text{M}_{\text{ML}}/\text{Pt}(111)$ conformation for all PtM alloys are likely to survive, where $\Delta E_{\text{segr}}(i)$ either stays

positive or is almost close to zero (dominate green and white colors, Figure 3). In H_2SO_4 solution, more thermoneutral $\Delta E_{\text{segr}}(i)$ are observed compared to the case of $HClO_4$ (Figure 3). Only PtOs retains highly positive $\Delta E_{\text{segr}}(i)$, while for PtCu, the segregation of Cu is thermodynamically favorable. In H_3PO_4 solution, $\Delta E_{\text{segr}}(i)$ for almost all PtM become negative, the thermoneutral $\Delta E_{\text{segr}}(i)$ is only observed for PtPd and PtIr, and slightly negative values for PtNi and PtRh (Figure 3). The effect of alkaline solution is similar as $HClO_4$. The presence of $*OH$ leads to the lowered $\Delta E_{\text{segr}}(i)$, but it is not significant enough to make the segregation of M highly exothermic. So the $Pt_{ML}/M_{ML}/Pt(111)$ conformation for all PtM systems can stay stable under the alkaline solutions.

3.3 Stability under the ORR condition.

The ORR is of great importance to the overall performance of low-temperature fuel cells. Therefore, we also studied the catalyst stability during the ORR. In our calculations, the effect of ORR on the segregation was modeled by considering the adsorption of reaction intermediates involved in the ORR. Despite the intensive effort expanded in studying fundamental problems of the ORR, many aspects of its kinetics are not well understood. ORR pathway is found to be similar in both acid and alkaline media on Pt-based catalysts.(34; 49) In aqueous solutions, the ORR appears to occur via two overall pathways: a four-electron pathway ($O_2 + 4H^+ + 4e^- \rightarrow 2H_2O$ in acid solutions; $O_2 + 2H_2O + 2e^- \rightarrow 4OH^-$ in alkaline solutions) and a peroxide or two-electron pathway ($O_2 + 2H^+ + 2e^- \rightarrow H_2O_2$).(34) The four-electron pathway is also proposed to run via two different mechanisms: direct mechanism ($O_2 + 2* \rightarrow 2O* + 2H^+ + 2e^- \rightarrow 2OH* + 2H^+ + 2e^- \rightarrow 2H_2O + 2*$) and associative mechanism ($O_2 + * \rightarrow O_2* + H^+ + e^- \rightarrow OOH* + H^+ + e^- \rightarrow H_2O + O* + H^+ + e^- \rightarrow H_2O + OH* + H^+ + e^- \rightarrow 2H_2O$).(41) Accordingly, the adsorptions of key intermediates including $*O$, $*OH$ and $*OOH$ were considered in our calculations.

*O interacts strongly with the surfaces by occupying the three-fold hollow sites. As shown in Figure 7a (also see Table S6), *O has a strong effect on the surface segregation, where $\Delta E_{\text{segr}}(i)$ for most PtM is highly negative. That is, the Pt_{ML}/M_{ML}/Pt(111) conformation is not stable anymore and the subsurface M is thermodynamically likely to segregate back to the surface due to the stronger interaction with *O than Pt. Again, the variation in $\Delta E_{\text{segr}}(i)$ depends on the E_d and therefore the activity of M toward *O according to extensive previous calculations. (40) For instance, the Fe with the highest-lying E_d (Figure S1) leads to the most significant changes in $\Delta E_{\text{segr}}(3)$ due to *O (4.46 eV). Positive or thermoneutral $\Delta E_{\text{segr}}(i)$ is only observed for PtCu and PtIr, and slightly negative values are obtained for PtRh and PtPd. In contrast, the effect introduced by *OH is much less. For all the systems studied, $\Delta E_{\text{segr}}(i)$ is either positive or close to zero (Figure 5d). In the case of *OOH, the situation is complicated (Figure 7b and Table S7). Depending on the surface composition, it can be adsorbed either molecularly on the atop position or dissociatively, where the *OH and *O fragments sit atop and hollow sites respectively (Figure 8). Our results show that the dissociative adsorption is energetically much more favorable than the molecular adsorption, which drives $\Delta E_{\text{segr}}(i)$ highly negative (Figure 7b). This is the case for PtFe, PtCo, PtRu, PtOs and PtIr (Figure 7b), where the segregation of M to the surface leads to the spontaneous O-O bond breaking. In the cases of PtNi, PtCu, PtRh and PtPd, *OOH stays as a molecule and $\Delta E_{\text{segr}}(i)$ remains positive.

According to our calculations, different alloying metals should be considered for the Pt-based catalysts to maintain the stability of Pt_{ML} on the surface depending on the undergoing ORR mechanisms. If the ORR follows the direct four-electron pathway via *O, Cu, Rh, Pd and Ir can be considered (Figure 3). Cu, Rh and Pd also work well if the reaction undergoes the associative four-electron pathway via both *O and *OOH (Figure 3). For those without *O but *OOH involved in the operating pathway, alloying with Ni, Cu, Rh and Pd should be able to hold the surface Pt_{ML}. In combination with the results on

solutions shown in section 3.2, the above predictions should also be valid for the ORR in HClO_4 , and alkaline solutions, where the effect of solution is not likely to vary the surface segregation significantly. In H_2SO_4 and H_3PO_4 solutions, Cu should be excluded, where the segregation of Cu to the surface is thermodynamically favorable.

Overall, PtRh and PtPd alloys are the only two systems, which display higher capability to keep the surface Pt_{ML} intact and therefore the catalyst stability under vacuum, various solutions and the ORR via different pathways. In addition, PtIr should also be paid attention, which only falls during the ORR via the $^*\text{OOH}$ intermediate. One common feature among the identified Pd, Rh and Ir is that they all locate next to Pt in the periodic table the metals with a E_{d} lying slightly higher than that of Pt. These metals are likely to provide the moderate binding, strong enough to hold the surface Pt_{ML} and weak enough to hinder the segregation induced by an adsorbate under the ORR conditions. Previous calculations have shown that the potential effect on the binding energy of an adsorbate is negligible even for the strong oxidant. (41) Accordingly, we expect that the predictions we presented here is likely to maintain under the working potential of the ORR.

Using the NSA model, our prediction on the stable alloys (PtRh, PtPd and PtIr) for the ORR can be synthesized in two possible ways in practice. One is simply as a core. Indeed, the higher stability of PtPd core-shell nanocatalysts have been reported experimentally for the ORR under various acid solutions.(13; 22) The other is as an interlayer between core and Pt shell.(10) In this case the core appropriate lattice structures can be selected to tune the surface strain and therefore the activity of Pt shells, while the interlayer containing Rh, Pd or Ir can contribute to promote the stability of Pt shell. Our results highlight the importance of chemical environments in affecting the stability of the catalysts.

4. Conclusion

DFT was employed to study the stability of various NSAs, $\text{Pt}_{\text{ML}}/\text{M}_{\text{ML}}/\text{Pt}(111)$,

under different conditions. Our results show that in vacuum conditions, the alloying M metals except Ag and Au thermodynamically prefer to stay in the subsurface and a Pt_{ML} is formed on the surface. The situation varies when considering the effect of solutions and the intermediates involved in the ORR via different pathways. In HClO₄ and alkaline solutions, the Pt_{ML}/M_{ML}/Pt(111) conformation is likely to survive when Pt forms alloys with Fe, Co, Ni, Cu, Ru, Rh, Pd, Os and Ir. PtCu in H₂SO₄ and PtM (M = Fe, Co, Cu, Ru, Os) in H₃PO₄ should be excluded, where Pt_{ML}/M_{ML}/Pt(111) is not likely to survive. This is due to the stronger interaction of anions with M than with Pt, which provides a big driving force to allow the segregation of M. Under the ORR via the direct four-electron pathway involving *O, alloying with Cu, Rh, Pd and Ir can be the candidates to achieve stability of surface Pt_{ML}. If it is via the associative four-electron pathway involving both *O and *OOH, only Cu, Rh and Pd can be considered. The Pt alloys with Ni, Cu, Rh and Pd can work well if the pathway only including *OOH rather than *O operates.

Overall, our calculations show that PtRh and PtPd alloys are the only two systems, being able to display higher stability under vacuum conditions, various solutions and the ORR via different pathways. In addition, PtIr should also be paid attention, which only falls during the ORR via the OOH intermediate. Our results highlight the importance of chemical environments in affecting the stability of the catalysts.

ACKNOWLEDGMENT

P.L. would like to thank the funding for the US Department of Energy, Office of Science under Contract No. DE-AC02-98CH10886, and W.T.Z. would like to thank the funding from National Natural Science Foundation of China (No. 51372095). The DFT calculations utilized resources at the Center for Functional Nanomaterials (CFN), Brookhaven National Laboratory and High Performance Computing Center, Jilin University.

References

- [1] D.J. Ham, J.S. Lee, *Energies* 2 (2009) 873-899.
- [2] A.-C. Dupuis, *Progress in Materials Science* 56 (2011) 289-327.
- [3] C.-Y. Wang, *Chem. Rev.* 104 (2004) 4727-4766.
- [4] F. Besenbacher, *Science* 279 (1998) 1913-1915.
- [5] N.M. Marković, P.N.R. Jr., *Surface Science Reports* 45 (2002) 117-229.
- [6] J.K. Norskov, C.H. Christensen, *Science* 312 (2006) 1322-3.
- [7] C. Wang, et al., *Nano Letters* 11 (2011) 919-926.
- [8] T. Ghosh, M.B. Vukmirovic, F.J. DiSalvo, R.R. Adzic, *J. Am. Chem. Soc.* 132 (2010) 906-907.
- [9] S.J. Yoo, H.Y. Park, T.Y. Jeon, I.S. Park, Y.H. Cho, Y.E. Sung, *Angewandte Chemie-International Edition* 47 (2008) 9307-9310.
- [10] K.A. Kuttiyiel, K. Sasaki, Y. Choi, D. Su, P. Liu, R.R. Adzic, *Energy & Environmental Science* 5 (2012) 5297-5304.
- [11] K.A. Kuttiyiel, K. Sasaki, Y. Choi, D. Su, P. Liu, R.R. Adzic, *Nano Letters* 12 (2012) 6266-6271.
- [12] K. Sasaki, H. Naohara, Y. Choi, Y. Cai, W.-F. Chen, P. Liu, R.R. Adzic, *Nat Commun* 3 (2012) 1115.
- [13] J.X. Wang, H. Inada, L. Wu, Y. Zhu, Y. Choi, P. Liu, W.-P. Zhou, R.R. Adzic, *J. Am. Chem. Soc.* 131 (2009) 17298-17302.
- [14] M.P. Hyman, J.W. Medlin, *Journal Of Physical Chemistry C* 111 (2007) 17052-17060.
- [15] J.K. Norskov, T. Bligaard, J. Rossmeisl, C.H. Christensen, *Nat Chem* 1 (2009) 37-46.
- [16] V. Stamenkovic, B.S. Mun, K.J. Mayrhofer, P.N. Ross, N.M. Markovic, J. Rossmeisl, J. Greeley, J.K. Norskov, *Angew Chem Int Ed Engl* 45 (2006) 2897-901.
- [17] H.Y. Su, X.H. Bao, W.X. Li, *Journal Of Chemical Physics* 128 (2008).
- [18] V.R. Stamenkovic, B.S. Mun, K.J.J. Mayrhofer, P.N. Ross, N.M. Markovic, *Journal Of the American Chemical Society* 128 (2006) 8813-8819.
- [19] G.E. Ramirez-Caballero, Y. Ma, R. Callejas-Tovar, P.B. Balbuena, *Phys Chem Chem Phys* 12 (2010) 2209-18.
- [20] J. Greeley, J. Rossmeisl, I.E.L.S. , I.C. , A.S. Bondarenko, J.K. Nørskov, T.P. Johansson, H.A.H. , T.F. Jaramillo, *Nature Chemistry* 1 (2009) 552-556.
- [21] W.J. Xu, D.J. Cheng, M. Niu, X.H. Shao, W.C. Wang, *Electrochimica Acta* 76 (2012) 440-445.
- [22] K. Sasaki, H. Naohara, Y. Cai, Y.M. Choi, P. Liu, M.B. Vukmirovic, J.X. Wang, R.R. Adzic, *Angewandte Chemie International Edition* 49 (2010) 8602-8607.
- [23] J. Greeley, J.K. Nørskov, *Electrochimica Acta* 52 (2007) 5829-5836.
- [24] J. Zhang, K. Sasaki, E. Sutter, R.R. Adzic, *Science* 315 (2007) 220-222.
- [25] J.X. Wang, C. Ma, Y.M. Choi, D. Su, Y.M. Zhu, P. Liu, R. Si, M.B. Vukmirovic, Y. Zhang, R.R. Adzic, *Journal of the American Chemical Society* 133 (2011) 13551-13557.
- [26] J. Greeley, M. Mavrikakis, *Catalysis Today* 111 (2006) 52-58.
- [27] J. Greeley, M. Mavrikakis, *Nat Mater* 3 (2004) 810-815.
- [28] M.D. Porosoff, W. Yu, J.G. Chen, *Journal of Catalysis* 308 (2013) 2-10.
- [29] A.S. Bandarenka, A.S. Varela, M. Karamad, F. Calle-Vallejo, L. Bech, F.J. Perez-Alonso, J. Rossmeisl, I.E.L. Stephens, I. Chorkendorff, *Angewandte Chemie International Edition* 51 (2012) 11845-

11848.

- [30] J.R. Kitchin, N.A. Khan, M.A. Barteau, J.G. Chen, B. Yakshinskiy, T.E. Madey, *Surface Science* 544 (2003) 295-308.
- [31] I.E.L. Stephens, et al., *Journal of the American Chemical Society* 133 (2011) 5485-5491.
- [32] J.B. Henry, A. Maljusch, M.H. Huang, W. Schuhmann, A.S. Bondarenko, *Acs Catalysis* 2 (2012) 1457-1460.
- [33] J. Knudsen, A.U. Nilekar, R.T. Vang, J. Schnadt, E.L. Kunkes, J.A. Dumesic, M. Mavrikakis, F. Besenbacher, *Journal of the American Chemical Society* 129 (2007) 6485-6490.
- [34] R.R. Adzic, in: J. Lipkowsky, P.N. Ross (Eds.), *Electrocatalysis*, New York, 1998, p. 197.
- [35] M.D. Segall, P.J.D. Lindan, M.J. Probert, C.J. Pickard, P.J. Hasnip, S.J. Clark, M.C. Payne, *J. Phys. Condens. Matter* 14 (2002) 2717-2744.
- [36] S.J. Clark, M.D. Segall, C.J. Pickard, P.J. Hasnip, M.I.J. Probert, K. Refson, M.C. Payne, *Z. Kristallogr* 220 (2005) 567-570.
- [37] J.P. Perdew, K. Burke, Y. Wang, *Phys. Rev. B* 54 (1996) 16533-16539.
- [38] B. Hammer, L.B. Hansen, J.K. Nørskov, *Phys. Rev. B* 59 (1999) 7413-7421
- [39] H.J. Monkhorst, J.D. Pack, *Physical Review B* 13 (1976) 5188-5192.
- [40] B. Hammer, J.K. Nørskov, *Advances in Catalysis* 45 (2000) 71.
- [41] J.K. Nørskov, J. Rossmeisl, A. Logadottir, L. Lindqvist, J. Kitchin, T. Bligaard, *J. Phys. Chem. B* 108 (2004) 17886-17892
- [42] A.S. Bondarenko, I.E.L. Stephens, H.A. Hansen, F.J. Perez-Alonso, V. Tripkovic, T.P. Johansson, J. Rossmeisl, J.K. Nørskov, I. Chorkendorff, *Langmuir* 27 (2011) 2058-2066.
- [43] N.M. Marković, R.R. Adžić, B.D. Cahan, E.B. Yeager, *Journal of Electroanalytical Chemistry* 377 (1994) 249-259.
- [44] H.N. Sharma, V. Sharma, T. Hamzehlouyan, W. Epling, A.B. Mhadeshwar, R. Ramprasad, *The Journal of Physical Chemistry C* 118 (2014) 6934-6940.
- [45] Q. He, X. Yang, W. Chen, S. Mukerjee, B. Koel, S. Chen, *Physical Chemistry Chemical Physics* 12 (2010) 12544-12555.
- [46] F. El Kadiri, R. Faure, R. Durand, *Journal of Electroanalytical Chemistry and Interfacial Electrochemistry* 301 (1991) 177-188.
- [47] A. Tanaka, K. Kanamura, A. R., B. Cahan, *Proceeding of Electrochemical Society Meeting, Montreal, 1990*, 969.
- [48] B.Z. NIKOLIC, R.R. ADZIC, *Journal of the Serbian Chemical Society* 62 (1997) 515-521.
- [49] N. Ramaswamy, S. Mukerjee, *Advances in Physical Chemistry* 2012 (2012) 17.

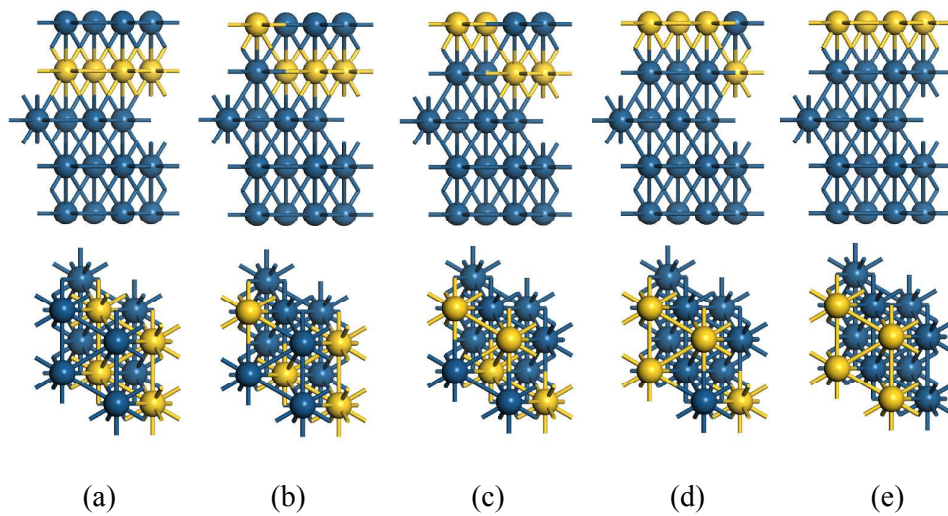


Figure 1 Optimized structures of NSA surfaces: (a) $\text{Pt}_4/\text{M}_4/\text{Pt}(111)$, (b) $\text{Pt}_3\text{M}_1/\text{Pt}_1\text{M}_3/\text{Pt}(111)$, (c) $\text{Pt}_2\text{M}_2/\text{Pt}_2\text{M}_2/\text{Pt}(111)$, (d) $\text{Pt}_1\text{M}_3/\text{Pt}_3\text{M}_1/\text{Pt}(111)$, (e) $\text{M}_4/\text{Pt}(111)$. Blue: Pt; yellow: M.

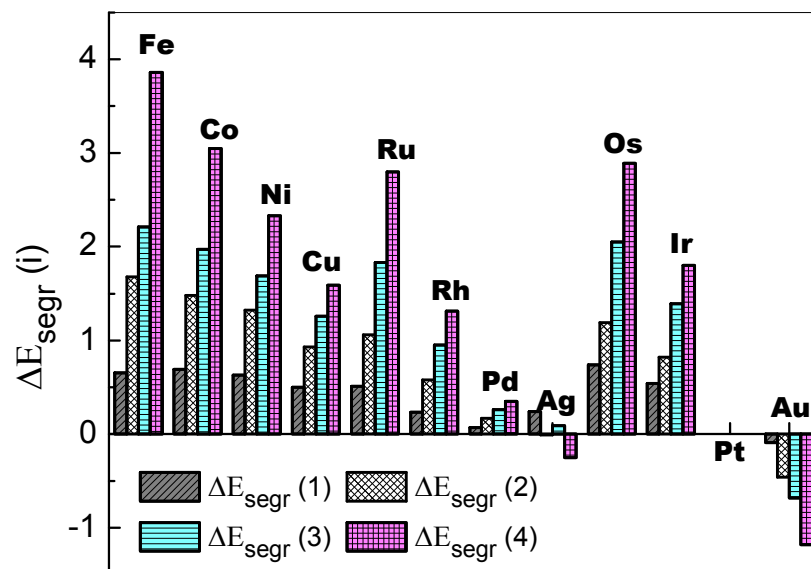


Figure 2 Calculated segregation energy, $\Delta E_{\text{segr}}(i)$, as a function of number of M on the surface of $\text{Pt}_4\text{M}_4/\text{Pt}(111)$.

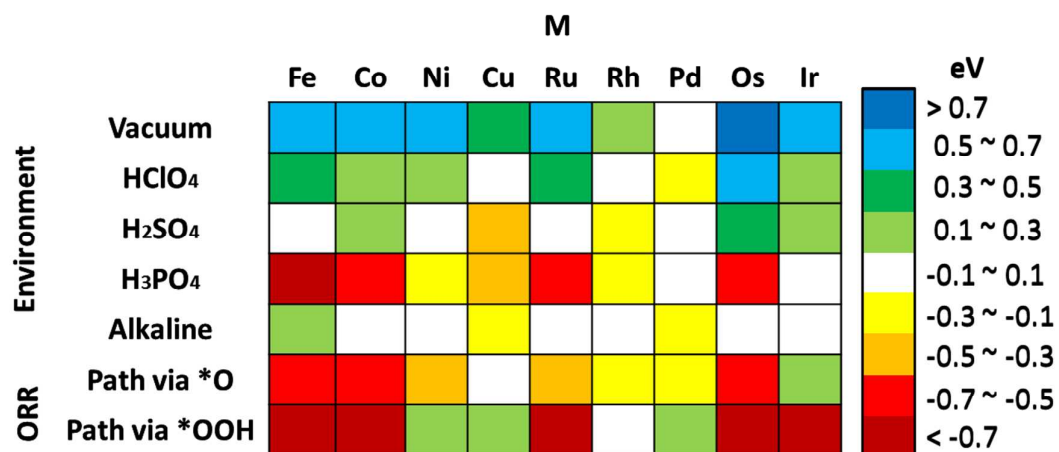


Figure 3 Color-labeled stability of the Pt_{ML} on various Pt_{ML}/M_{ML}/Pt(111) surfaces under various conditions. Color index scale the stability from high (dark blue) to low (dark red) according to the lowest $\Delta E_{\text{segr}}(i)$ calculated using DFT.

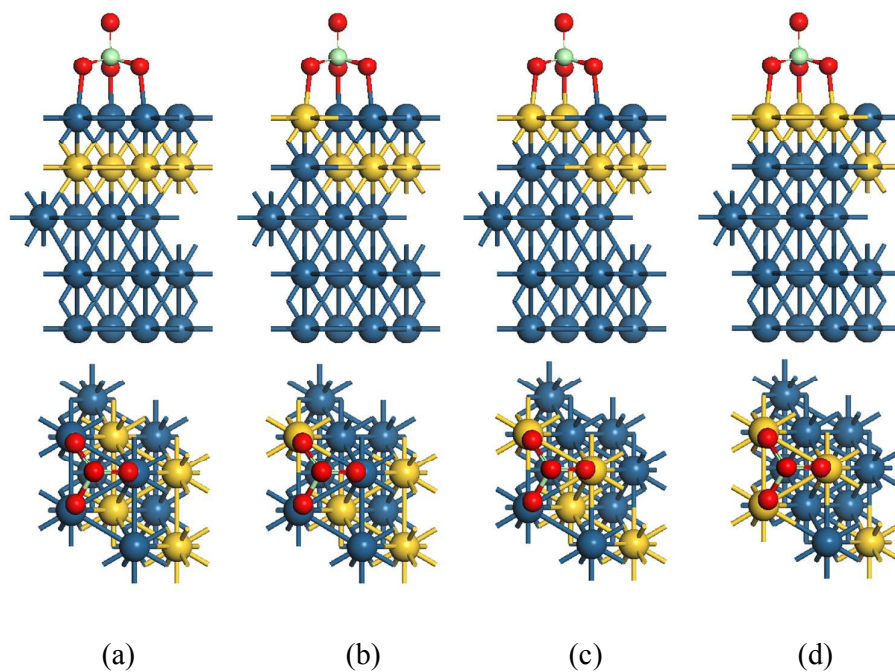


Figure 4 Optimized structures of $^*\text{ClO}_4$ on the NSA surfaces: (a) $\text{Pt}_4/\text{M}_4/\text{Pt}(111)$, (b) $\text{Pt}_3\text{M}_1/\text{Pt}_1\text{M}_3/\text{Pt}(111)$, (c) $\text{Pt}_2\text{M}_2/\text{Pt}_2\text{M}_2/\text{Pt}(111)$, (d) $\text{Pt}_1\text{M}_3/\text{Pt}_3\text{M}_1/\text{Pt}(111)$. Blue: Pt; yellow: M; red: O; green: Cl.

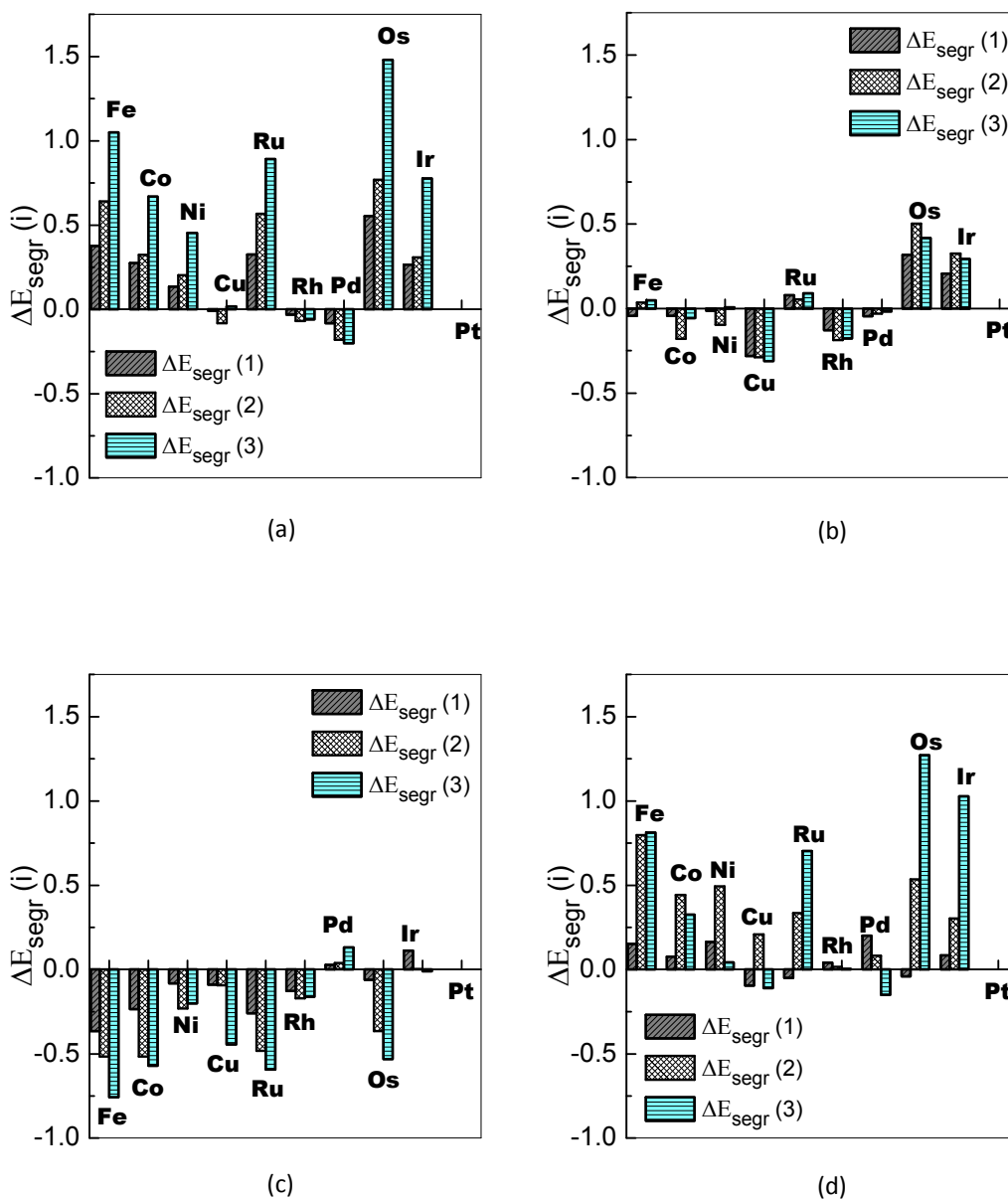


Figure 5 Calculated segregation energy, $\Delta E_{\text{segr}}(i)$, as a function of number of M on the surface of $\text{Pt}_4/\text{M}_4/\text{Pt}(111)$ in HClO_4 (a), H_2SO_4 (b), H_3PO_4 (c) and alkaline (d) solutions.

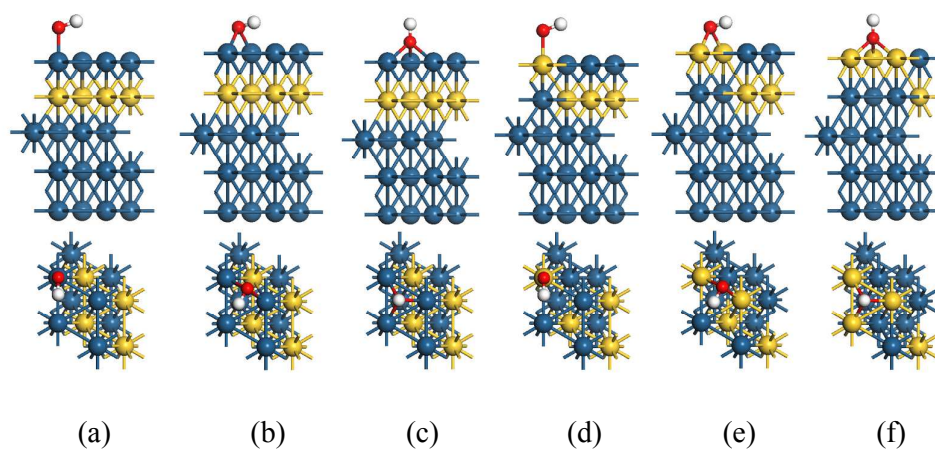


Figure 6 Optimized structures of *OH on the NSA surfaces: (a,b,c) $\text{Pt}_4/\text{M}_4/\text{Pt}(111)$, (d) $\text{Pt}_3\text{M}_1/\text{Pt}_1\text{M}_3/\text{Pt}(111)$, (e) $\text{Pt}_2\text{M}_2/\text{Pt}_2\text{M}_2/\text{Pt}(111)$, (f) $\text{Pt}_1\text{M}_3/\text{Pt}_3\text{M}_1/\text{Pt}(111)$. Blue: Pt; yellow: M; red: O; white: H.

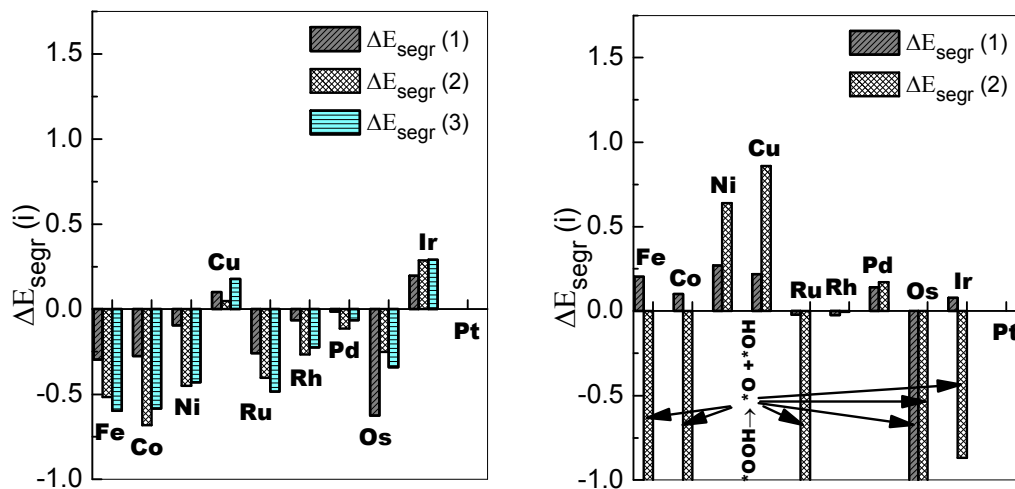


Figure 7 Calculated segregation energy, $\Delta E_{\text{segr}}(i)$, as a function of number of M on the surface of $\text{Pt}_4/\text{M}_4/\text{Pt}(111)$ under the ORR condition: (a) *O ; (b) *OOH .

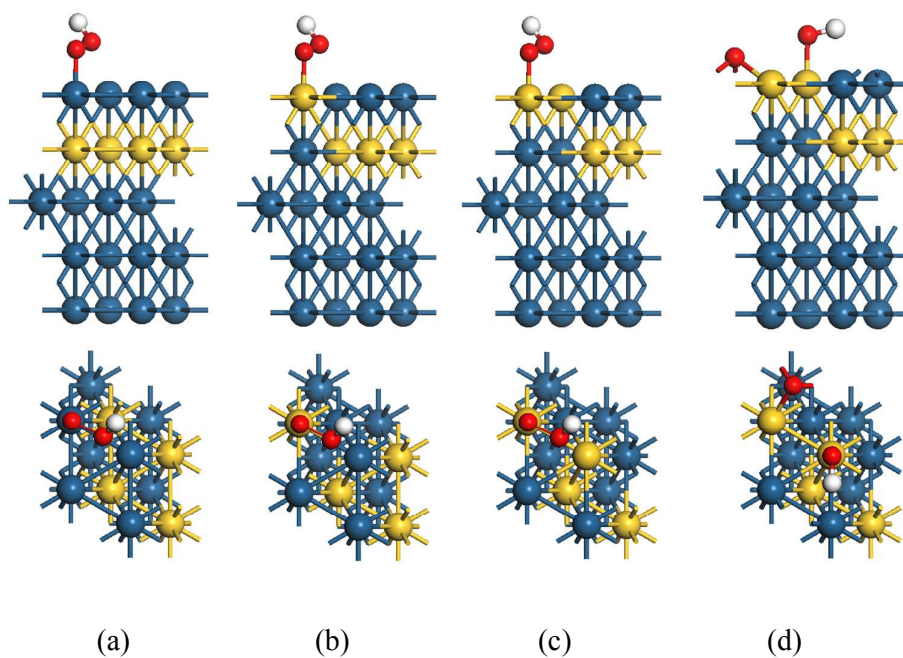


Figure 8 Optimized structures of $*OOH$ molecularly on (a) $Pt_4/M_4/Pt(111)$, (b) $Pt_3M_1/Pt_1M_3/Pt(111)$, (c) $Pt_2M_2/Pt_2M_2/Pt(111)$ and dissociatively to $*O$ and $*OH$ on (d) $Pt_2M_2/Pt_3M_1/Pt(111)$. Blue: Pt; yellow: M; red: O; white: H.

TOC

